Free-Surface Effects on Two-Dimensional Hydrofoils by RANS-VOF Simulations

Laetitia Pernod, Matthieu Sacher, Jeroen Wackers, Benoit Augier, Patrick Bot

Journal of Sailing Technology 2023, volume 8, issue 1, pp. 24 –38.
The Society of Naval Architects and Marine Engineers.

Free-Surface Effects on Two-Dimensional Hydrofoils by RANS-VOF Simulations

Laetitia Pernod
IRENav, Ecole Navale, 29240 Brest, France

Matthieu Sacher
ENSTA Bretagne, CNRS UMR 6027, 29200 Brest, France

Jeroen Wackers
LHEEA, Ecole Centrale de Nantes, CNRS UMR 6598, 44300 Nantes, France

Benoit Augier
IFREMER, 29200 Brest, France.

Patrick Bot
IRENav, Ecole Navale, 29240 Brest, France, patrick.bot@ecole-navale.fr

Manuscript received October 13, 2022; revision received January 5, 2023; accepted January 22, 2023.

Abstract. Foiling yachts and crafts are both very sensitive to the flying height in terms of stability and performance, raising the scientific issue of the influence of the free-surface when the foil is at low submergence. This work presents numerical simulations of a 2D hydrofoil section NACA0012 at 5° angle of attack in the vicinity of the free-surface, for different values of the submergence depth, for a chord-based Froude number of 0.571 and a Reynolds number of 159,000. Unsteady-Reynolds Averaged Navier-Stokes (URANS) equations are solved with a mixture model to capture the free surface (Volume Of Fluid method), and using an automatic grid refinement. Verification of the numerical model and validation with data from the literature are presented. Deformation of the free surface and alteration of the hydrodynamic forces compared to the deep immersion case are observed for a submergence depth-to-chord ratio h/c lower than 2. The foil drag increases up to more than three times the infinite-depth value at $h/c \approx 0.5$. The lift force slightly increases until h/c around 1, and then decreases sharply. For $h/c < 0.5$, the pressure field around the foil is totally modified and the lift is swapped to downward. The study highlights the importance of considering the effect of finite submergence to compute foils' hydrodynamic forces, for example to be used in Velocity Prediction Programs (VPP) of foiling crafts.

Keywords: Hydrofoils; Free Surface; URANS; VOF; Submergence depth; Froude number.

NOMENCLATURE

$A_{\max}$	Maximum free-surface elevation [m]
$A_{\min}$	Minimum free-surface elevation [m]
c	Chord length [m]
C_D	Drag coefficient [-]
C_L	Lift coefficient [-]
F_r	Froude number (chord-based $F_r = U_\infty \sqrt{gc}$) [-]
g	Acceleration of gravity [m s^{-2}]
h	Submergence depth [m]
p	Pressure field [Pa]
t	A time instant [s]

T_r	Grid Refinement threshold [m]
U	Flow velocity [m s^{-1}]
U_∞	Incoming flow velocity [m s^{-1}]
(x, y)	Cartesian coordinates [m]
y^+	Dimensionless wall distance [-]

α	Angle of attack [°]
Δt	Time step [ms]
$\varepsilon_{\mathrm{CD}}$	Relative error in the drag coefficient [%]
$\varepsilon_{\mathrm{CL}}$	Relative error in the lift coefficient [%]
η	Free-surface elevation [m]
λ	Wavelength [m]
ρ	Fluid density [kg m^{-3}]

CFD	Computational Fluid Dynamics
FVM	Finite Volume Method
IRENav	Institut de Recherche de l'Ecole Navale
URANS	Unsteady-Reynolds Averaged Navier-Stokes
VOF	Volume of Fluid
VPP	Velocity Prediction Program

1. INTRODUCTION

Applications for hydrofoils in marine engineering, such as racing sailing boats and fast passenger ferries, are progressively expanding and gaining economic importance. Indeed, these appendages are used to generate lift to partially or fully support a ship's weight, thus reducing the hydrodynamic resistance, as a significant fraction of the ship's hull is lifted out of the water (Buerman *et al.*, 1953; Molland 2008). The use of lifting hydrofoils as a means of drag reduction has caused a jump in yacht performance and increased velocities over the recent years. A recent example is given by Patterson and Binns (2022) who developed a six degree of freedom Velocity Prediction Program for the foiling America's Cup vessels.

Hydrofoils typically operate in proximity to the free-surface, being either fully but shallowly submerged or surface-piercing, such as rudders, kitefoils' and windfoils' masts, struts, etc., (see classical classification of hydrofoils in Faltinsen 2005; Molland 2008) and this significantly alters the dynamics of the flow field compared to unbounded flow (Xie and Vassalos 2007; Bal 2007). When a foil moves closely beneath a free-surface, the low pressure zone existing on its suction side acts to deform the free-surface, hence generating a transverse wave following the foil (Parkin *et al.*, 1956; Duncan 1983). The subsequent hydrodynamic coefficients and wave pattern behavior is less understood. Indeed, on the one hand, some researchers observed that the induced wave field creates an additional drag component due to the wave resistance, and curves the flow, leading to a decrease of the foil's effective camber, hence reducing lift when the foil moves closer to the free-surface (Parkin *et al.*, 1956; Daskovsky 2000; Filippas and Belibassakis 2014; Prasad *et al.*, 2015; Ni *et al.*, 2021). This dynamic mechanism of lift reduction seems to be amplified by shallow submergence. On the other hand, it was shown that under certain conditions of velocity (Froude number) and submergence depth ratio (h/c), the lift force may increase when the foil is getting closer to the free-surface (Hough 1969; Ali and Karim 2010; Karim *et al.*, 2014; Hoque *et al.*, 2017), or the wave pattern may become drastically different (Parkin *et al.*, 1956; Yeung and Bouger 1979; Duncan 1983).

Based on these findings, the influence of the free-surface on the foil's hydrodynamic performance appears to be strongly dependent on the dominant problem parameters (Froude number, submergence depth to chord ratio and angle of attack), and seems to alternate between lift reduction and augmentation (Xie and Vassalos 2007; Ozdemir*et al.*, 2021). Furthermore, while

several studies addressed the relatively complex flow phenomena related to the interaction between the induced-wave train and the flow surrounding the hydrofoil, the relationship between the nature of the flow regime (and thus its consequences on the hydrodynamic coefficients and wave pattern) and the dominant problem parameters, is not yet fully understood. Consequently, and due to their increasing popularity, it becomes more and more important to accurately understand the physics of foilers, and to consider the effects of finite submergence depth on the performance in the numerical modeling. Bagué *et al*. (2021), for example, applied CFD to analyze the dynamic stability of a sailing foiler, but did not consider the alteration of foil forces due to the proximity of the free surface.

The purpose of this paper is to setup and validate a numerical method that will later be used for an extensive investigation of free-surface effects on a submerged hydrofoil moving closely beneath a free-surface. As such, this work represents the first step of a more complete study. The first section describes the numerical model, which is based on a Unsteady-Reynolds-Averaged-Navier-Stokes (URANS) approach closed by the classical *k*-*ω*-SST turbulence model, and associated to a capturing interface method to represent the free-surface. The considered geometry, boundary conditions and numerical parameters are also presented in this first section. Then, CFD verification and validation are carried out: the verification includes mesh and time convergence, while the validation provides comparison of free-surface deformation and hydrodynamic coefficients for different submergence depth to chord ratios against experimental and numerical data from the literature. Finally, an in-depth analysis of the pressure field surrounding the hydrofoil gives some insights into the physics of free-surface effects.

2. NUMERICAL MODEL

2.1. Numerical Framework

The fluid problem is modelled and solved using the CFD computational suite FINE/Marine version 10.1, commercialized by CADENCE (formerly NUMECA), and based on the flow solver ISIS-CFD developed by Ecole Centrale de Nantes (Nantes, France). ISIS-CFD is used to solve the equations closed by the *k*-*ω*-SST turbulence model by Menter (Menter *et al.*, 1994). All the viscous computations are made using a URANS low-Reynolds boundary-layer resolution method ($y^+ \leq 1$). Moreover, the free-surface is captured by a mixture-model approach to represent the interface between the two phases of air and water (Queutey and Visonneau 2007). Details for the practical implementation of the turbulence closure in FINE/Marine, and the associated relevant numerical parameters, may be found in the official documentation (METHRIC 2020).

The spatial discretization of the fluid computational domain is achieved using Finite Volume Method (FVM) with an unstructured hexahedral mesh generated by the meshing software HEXPRESS, included in FINE/Marine computational suite. Furthermore, an automatic and anisotropic grid adaptation is performed using a combined free-surface and pressure criterion, in order to accurately capture the free-surface deformation and accurately model the boundary layer surrounding the foil (Wackers *et al.* 2017; METHRIC 2020). The free-surface criterion consists in directly prescribing the cell size at the free-surface interface, in a direction normal to the water interface. The pressure criterion is based on the Hessian matrix of second derivatives of the pressure. The criteria are applied in a metric context: the mesh is refined until the product of the criteria and the cell sizes is approximately constant throughout the mesh. Thus, high values of the criterion lead to small cells. Finally, temporal discretization is achieved through a second-order-implicit backward Euler scheme.

2.2. Geometry, Configuration and Reference Data

The numerical model is validated against experimental and numerical data presented in the literature, in order to assess its capability concerning the accurate modelling of free-surface deformation due to a moving foil, and the influence of free-surface effects on the hydrodynamic coefficients. Experimental data is taken from the work of Duncan (Duncan 1983), who performed

towing-tank experiments on a NACA0012 - aluminum hydrofoil operating at 5° angle of attack and different submergence depths h to chord c ratios, in the range $0.78 < h/c < 1.29$. The hydrofoil chord length is $c = 0.203$ m, with a 12% relative thickness at 30% of the chord. Moreover, hydrofoil span (0.6 m) is almost equal to the width of the towing tank (0.61 m), and consequently, the problem may be considered two-dimensional. However, infinite depth condition cannot be considered because the hydrofoil is located only 0.175 m above the bottom of the towing tank, corresponding to $0.875c$. Finally, the hydrofoil towing speed is 0.8 m/s, corresponding to a rather low Froude number of 0.571 (based on the chord) and moderate Reynolds number of 159,000.

Unfortunately, the hydrodynamic forces were not measured, but Duncan's experimental work is used as a reference in several subsequent studies. In particular, the hydrodynamic coefficients of lift and drag are computed along with the free-surface deformation, by Ali and Karim (2010) and Prasad *et al.* (2015).

2.3. Numerical Setup

The fluid domain used in the computations is presented on Fig. 1, with the origin of the coordinate system set at the leading edge of the hydrofoil. Water has a density of 1027 kg m^{-3} and a dynamic viscosity of 0.001397 Pa s.The fluid domain is specified relatively to the number of chord lengths upstream ($10c$), downstream ($20c$), above ($5c$) and below ($0.875c$) the foil: the dimensions are chosen in order to avoid confinement effects due to the boundaries, to the exception of the bottom boundary. Indeed, as mentioned in the previous sub-section, the hydrofoil is located close to the bottom of the towing tank, and shoaling effects are thus non-negligible. Therefore, the finite depth is reproduced in the computation using the experimental value of $0.875c$ below the hydrofoil, and a slip condition is imposed on the bottom boundary ($y = y_{\min}$, condition 3 on Fig. 1). A pressure condition is set on the top ($y = y_{\max}$) and outlet boundaries ($x = x_{\max}$) in the form of a Dirichlet condition with an updated hydrostatic pressure (condition 2 on Fig. 1):

$$p(x_{max}, y, t) = -\rho g(\eta(x_{max}, t) - y), \tag{1}$$

meaning that the prescribed value for the pressure on the boundary will evolve during the computation according to the free-surface position. The last external patch (inlet $x = x_{\min x}$) is set to a far-field condition, that is, a Dirichlet condition on the velocity: the incoming flow has a velocity U_∞ (condition 1 on Fig. 1). Finally, a no-slip condition is enforced on the foil's surface (zero-velocity at the boundary, condition 4 on Fig. 1). Initially, the fluid and free-surface are considered at rest (zero-velocity in the whole computational domain, the foil is accelerated up to the prescribed velocity with a ramp of 200 time steps), and the position of the interface is defined through the immersion depth h between the initial position of the interface and the position of the center-line at mid-chord ($c/2$ and not the origin of the coordinate system, in order to compare to the literature): $\eta(x, t_0 = 0) = h$.

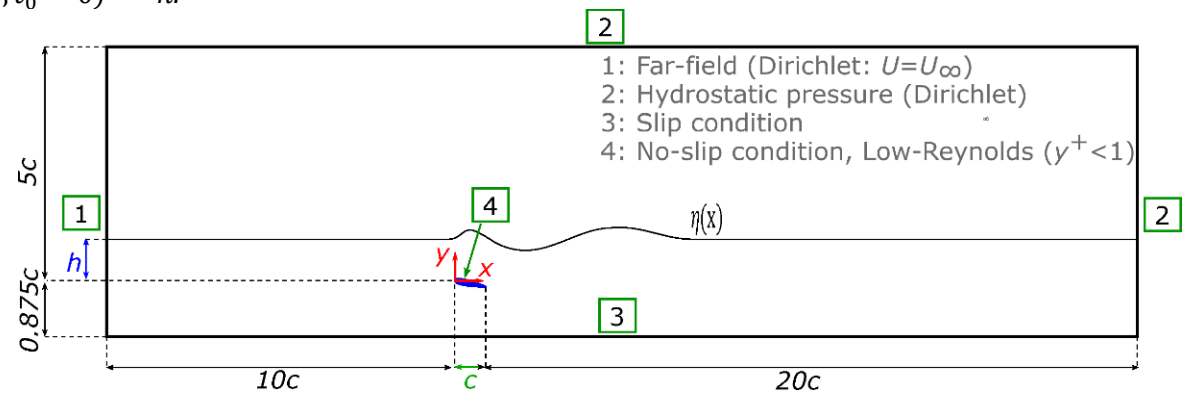

Figure 1. Schematic of the fluid domain and its boundary conditions.

2.4. Verification: Mesh and Time Convergence

To produce a grid-independent solution, that is, a solution with small enough spatial discretization errors due to interpolation and approximate integration, a grid convergence study is performed on five different meshes using the following method:

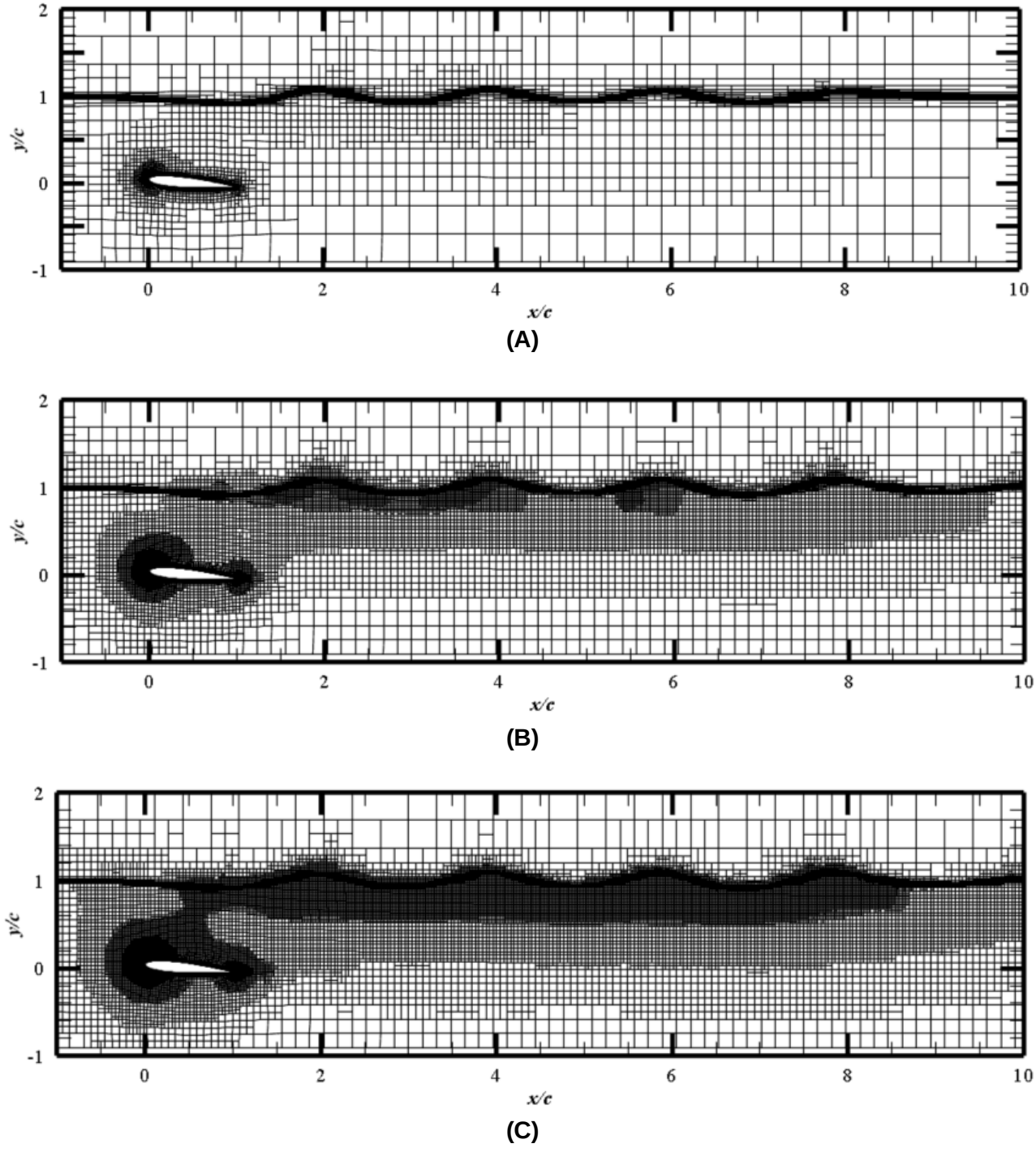

Figure 2. Mesh topology for pressure Hessian refinement (A) $T_r/c = 0.2$**, (B)** $T_r/c = 0.07$ **and (C)** $T_r/c = 0.05$**.**

- First, a coarse mesh is created to serve as a common initial mesh to all five meshes in the Series.
- The target grid size for cells normal to the free-surface (i.e. the cell size at the free-surface, corresponding to the free-surface criterion of the automatic refinement technique) is set at

$c/100$ (2 10^{-3} m).

- Minimum cell size set at $c/1000$ (2 10^{-4} m).
- For each mesh, the Hessian threshold T_r is divided by $\sqrt{2}$ with respect to the previous mesh (thus, the cell sizes are halved every two meshes), for values ranging from 0.2 to 0.05.
- Then, the computations are made with strict tolerances for iterative convergence (1%), to enforce minimization of iterative convergence errors.

Wackers *et al.* (Wackers *et al.* 2017), proved that such a method of grid convergence study can indeed produce grid-independent solution and be used for uncertainty estimation. The grid convergence study is carried out for a 5° angle of attack, a chord-based Froude number $F_r = U_\infty\sqrt{gc}) = 0.571$(corresponding to $U_\infty =$ 0.8 m s^{-1}) and an immersion depth of one chord length ($h/c = 1.03$). Figure 2 shows the topology of the coarsest mesh $T_r/c = 0.2$ (A), the finest mesh $T_r/c = 0.05$ (C) and an intermediary mesh $T_r/c = 0.07$ (B). Local refinements at the free-surface and in the boundary layer surrounding the hydrofoil are clearly visible, with smaller and more numerous cells when the threshold is decreasing (12,681 cells for the coarsest mesh (A), 45,767 cells for the intermediary mesh (B) and 69,419 cells for the finest mesh (C)). Moreover, the meshes are geometrically similar, as the different levels of refinement start roughly at the same value for x/c and y/c.

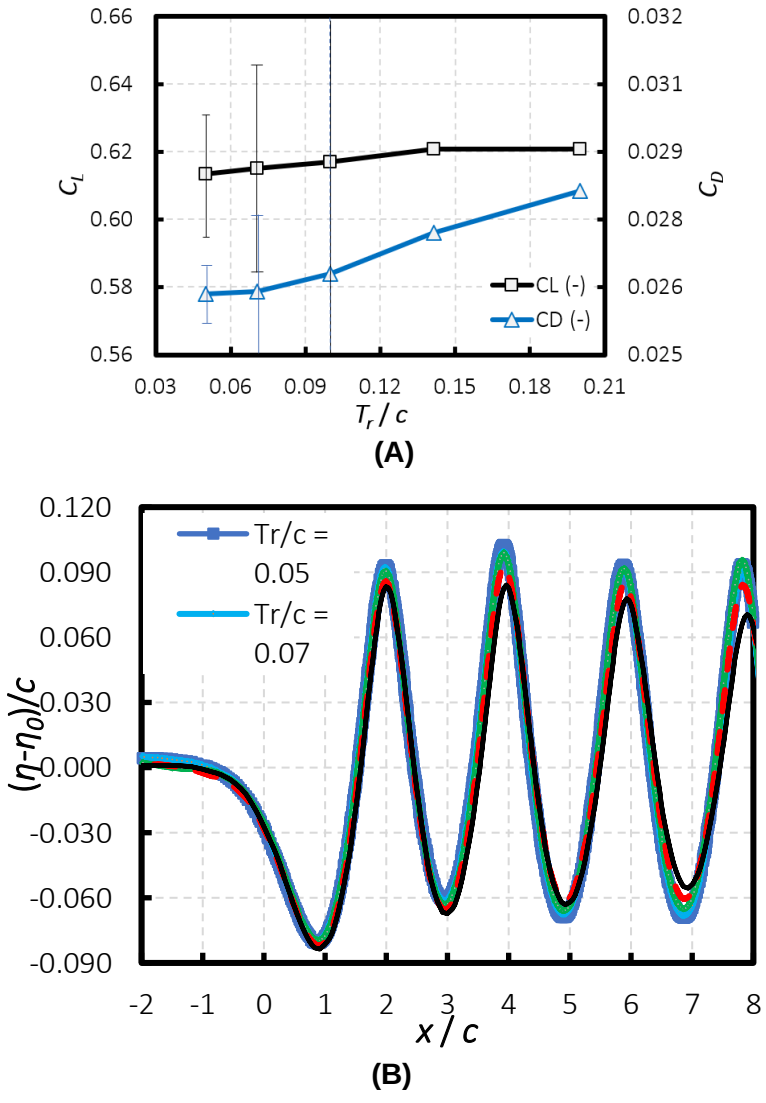

Figure 3. Grid convergence with respect to the grid refinement threshold T_r/c (the lower the threshold, the finer the mesh) of (A) lift and drag coefficients and (B) free-surface deformation.

Figure 3A presents the grid convergence of lift and drag coefficients for the hydrofoil, with respect to the threshold to chord ratio T_r/c (the lower the ratio, the finer the mesh). Error bars show the uncertainty estimation for the finest grid using the methodology by Eça and Hoekstra (2014): the uncertainty is estimated at 3% for the lift, and 2% for the drag. Grid convergence on the free-surface deformation is visible on Figure 3B. For the subsequent investigation, the refinement criterion of the fourth mesh is chosen, corresponding to a threshold to chord ratio $T_r/c = 0.07$, and a difference with the finest mesh ($T_r/c = 0.05$) of 0.26% for the lift coefficient, 0.22% for the drag coefficient and no visible difference on the free-surface deformation.

A time convergence study is then carried out for five different time steps, each divided by 2 relative to the previous time step. Table 1 presents the values of lift and drag coefficients for the time convergence study, associated with the relative difference. A time step of 10 ms is selected.

Table 1. Time convergence study.

Δt (ms)	C_L (-)	C_D (-)	$\varepsilon_{\mathrm{CL}}$ (%)	$\varepsilon_{\mathrm{CD}}$ (%)
1.3	0.6141	0.0266	-	-
2.5	0.6138	0.0265	-0.06	-0.36
5.1	0.6132	0.0265	-0.15	-0.33
10	0.6127	0.0265	-0.24	-0.24
20	0.6056	0.0272	-1.40	2.25

3. RESULTS

3.1. Validation: Free-Surface Deformation for Different Submergence Depths

After a suitable mesh and numerical parameters have been selected, results are first validated against the experimental data of Duncan in 1983. Figure 4 shows a comparison between measured (red/gray squares) and simulated (black solid line) free-surface deformation η for different values of the submergence depth to chord ratio. The foil is located between $x/c = 0$ and $x/c = 1$ for all the conditions, only the immersion depth changes. First, concerning the physical processes involved, one may observe that the influence of the submergence depth on the free-surface deformation is very similar to a “ground effect” or “shoaling” effect. Indeed, as the foil gets closer to the free-surface, the wave height increases and the waves become sharper, resulting in the development of non-linearities and finally wave breaking, when the camber reaches its physical limit.

Now, regarding the numerical to experimental comparison, for (A) $h/c = 1.29$, (B) $h/c = 1.16$ and (C) $h/c = 1.03$, the numerical results are qualitatively very consistent with the experimental results (Figure 4 A, B and C). The difference between the experimental data and the numerical results is below 6.5% for the wavelength and around 10% for the crest-to-trough amplitude of the front-wave. Then, for (D) $h/c = 0.95$, the discrepancies on the wavelength are increased up to 8%, while the crest-to-trough amplitude is decreased to 4%. However, the wave camber seems to become sharper than the experimental results, even though the global free-surface elevation shape still qualitatively agrees very well with the experimental data (Figure 4 D).

Finally, when non-linearities due to the front-wave breaking start developing, for (E) $h/c = 0.911$ and (F) $h/c = 0.78$, the difference between the experimental and numerical results increases (Figure 4 E and F): the front-wave shape is mis-reproduced, as the camber is over-exaggerated by the simulation, and is even reversed to take the shape of a roller, while it is not the case experimentally. On the contrary, the slope of the preceding trough is under-estimated, and the trough starts further downstream from the foil. However, the crest-to-trough amplitude of the first trough matches very well, with less than 1% difference for $h/c = 0.91$, and the amplitude and wavelength of the following wave-train are qualitatively well represented.

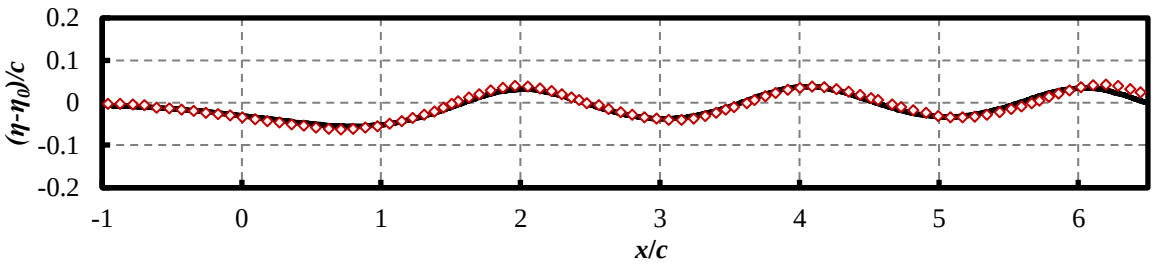

(A) $h/c = 1.29$

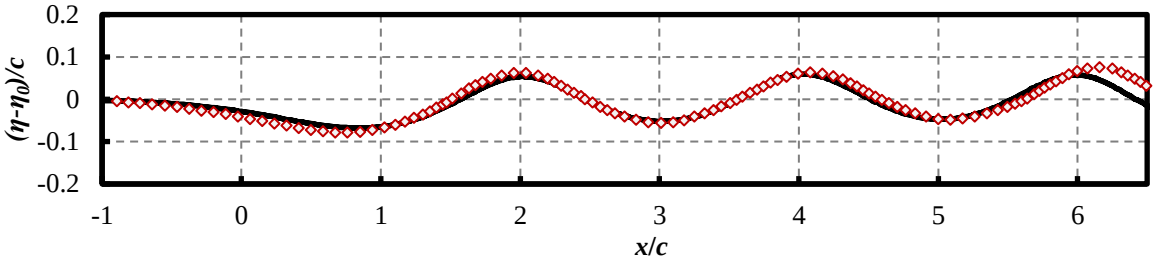

(B) $h/c = 1.16$

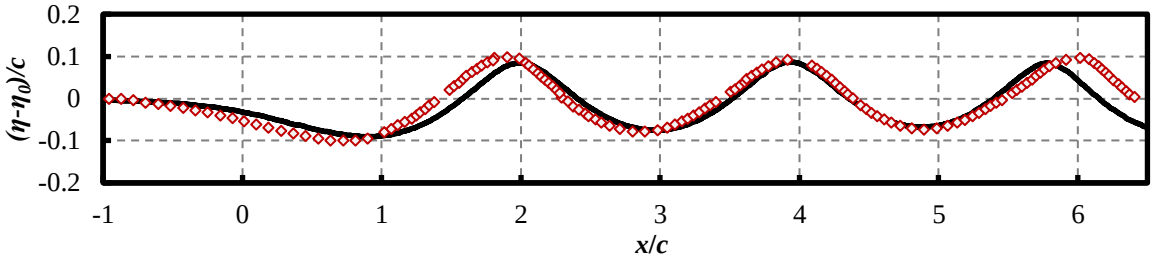

(C) $h/c = 1.03$

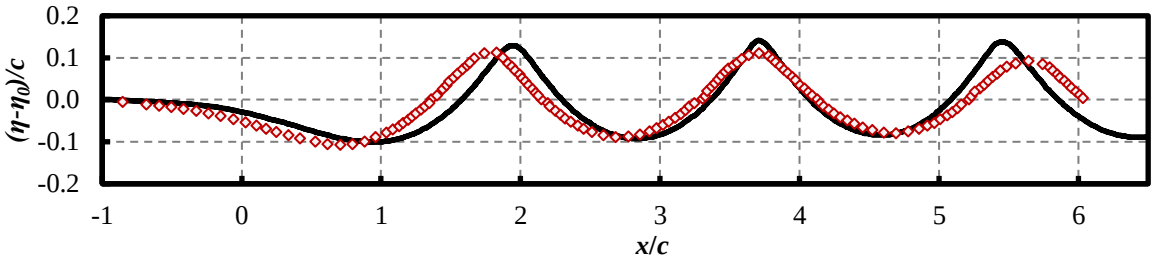

(D) $h/c = 0.95$

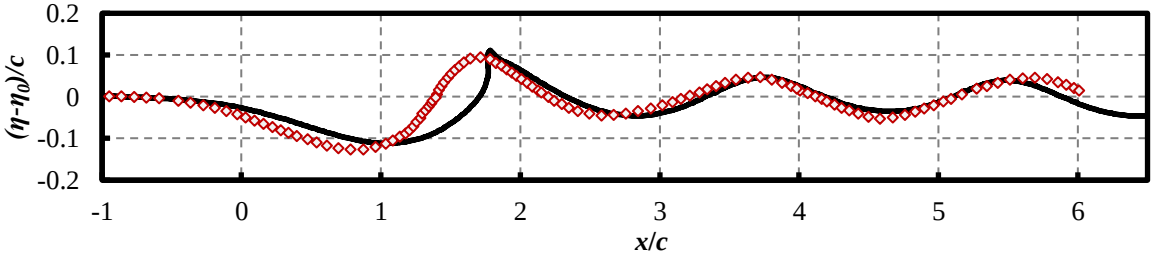

(E) $h/c = 0.911$

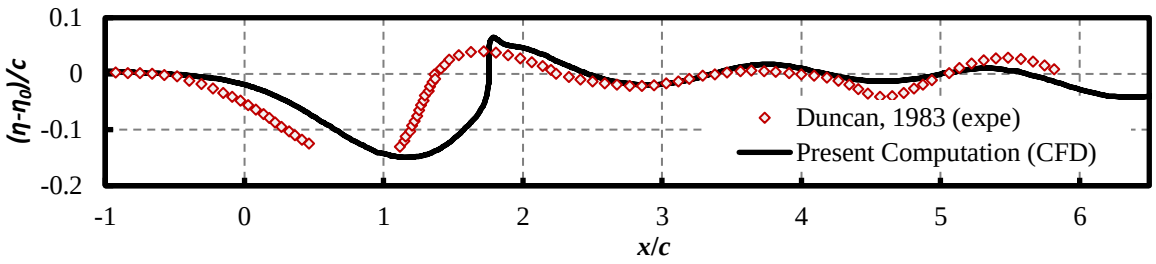

(F) $h/c = 0.78$

Figure 4. Comparison of free-surface deformation between experimental data (red/gray squares) from Duncan (1983) and the present computation (black solid line) for different submergence depth to chord ratios. The hydrofoil is located under the free-surface between $x/c = 0$ and $x/c = 1$.

It should be noted that when wave breaking occurs (for $h/c \leq 0.911$), the results become unsteady and the free surface position is not well defined (present computation in Fig. 4 and 5 show the computed instantaneous wave profiles). It is expected that rather similar limitations apply to the experimental results, where determining the free-surface position in the foam is likely to be difficult. No information is provided about the temporal evolution in the results from the literature.

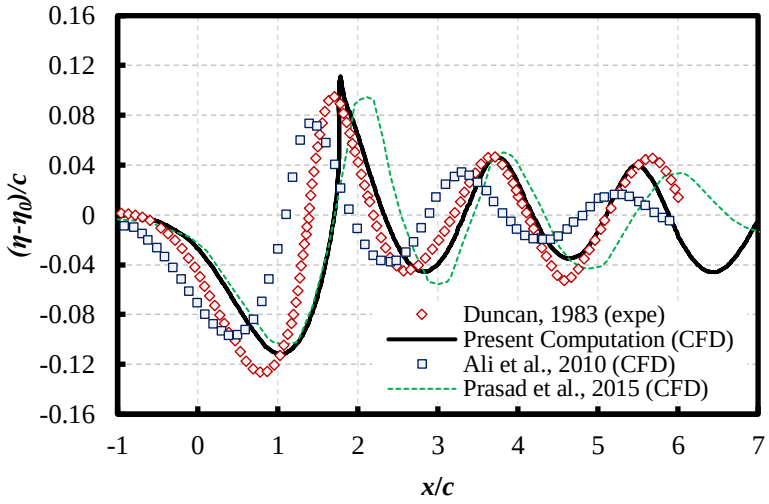

Figure 5. Comparison of free-surface deformations between experimental data from Duncan (1983), numerical data from Ali and Karim (2010) and Prasad *et al.* (2015) and the present computation for $h/c = 0.911$. The hydrofoil is located under the free-surface between $x/c = 0$ and $x/c = 1$.

All in all, the free surface elevation predicted by the numerical model agrees very well with the experimental free surface position for a submergence depth to chord ratio down to 1, and reasonably well for lower submergence except that the first trough is not accurately located. To be more quantitative and determine the range of applicability of our model, we now look at hydrodynamic forces. The experimental results of Duncan do not include force measurements; however, numerical simulations by Ali and Karim (2010) and Prasad *et al.* (2015) include the computation of the hydrodynamic coefficients along with the validation of the free-surface deformation compared to Duncan's results. As a consequence, for the condition $h/c = 0.911$ (which is the only common submergence depths to all four approaches), the computed free-surface deformation (black solid line) is also compared to the numerical results of Ali and Karim (2010) (blue/gray squares) and Prasad *et al.* (2015) (green dotted line) on Fig. 5. Experimental results of Duncan are also represented on the figure for reference (red/gray squares). Moreover,

the maximum and minimum heights (respectively $A_{\max}$ and $A_{\min}$) of the free-surface deformation, corresponding respectively to the front-wave height and the depth of the preceding trough, are compared in Table 2 for the different numerical simulations and the experimental data. The wavelength λ, measured between the second and third crests, is also compared in the same table (the first crest is not always well defined because of wave breaking).

Table 2. Comparison of maximum and minimum surface elevation and wavelength for $h/c = 0.911$.

	$A_{\max}/c$	$A_{\min}/c$	h/c	λ/c
Duncan, 1983	0.0953	-0.1262	0.2215	1.97
Ali and Karim, 2010	0.0738	-0.0961	0.1699	1.91
Prasad et al., 2015	0.0948	-0.1039	0.1987	2.20
Present computation	0.1112	-0.1117	0.2229	1.79

In the simulation by Ali and Karim (2010), the non-linearities are under-estimated, and the absolute values of the maximum and minimum surface elevations are also under-estimated (by 22.5% and 23.8%, respectively, corresponding to a crest-to-trough difference of 23.3%). In addition, the increased sharpness of the front-crest is not modeled, and the amplitudes of the following wave-train are over-damped, but the wavelength is rather well-represented (under-estimation of 2.8%). On the contrary, Prasad *et al.* (2015) very accurately reproduce the first-crest maximum amplitude, with only 0.5% difference, and a lower difference of 17.6% on the minimum in the trough, corresponding to a crest-to-trough difference of 10.3%. However, the wavelength is over-estimated by 11.6%, and the amplitudes of the following wave-train are also over-damped. Finally, the present simulation represents an accurate numerical prediction of the free-surface deformation, concerning both the increased sharpness of the first-crest, the maximum and minimum surface elevation (over-prediction of 16.8% and under-prediction of 11.5%, respectively, in this condition $h/c = 0.911$, corresponding to a crest-to-trough difference of only 0.65%), the wavelength underprediction of 8.9%) and the amplitudes of the following wave-train. Furthermore, it should be noted that i) simulations by Prasad *et al.* (2015) and Ali and Karim (2010) consider a higher depth between the hydrofoil and the bottom boundary, while this work represents the depth effects of the finite depth in Duncan's experiments, and ii) this condition ($h/c = 0.911$) is one of the most difficult to validate with the numerical models, because of the existence of wave-breaking and the associated nonlinearities: these results are thus considered to agree well with the experimental and numerical data, with a greater confidence of accuracy for moderate to high h/c ($h/c > 1$) and a lower confidence for low h/c ($h/c < 1$).

3.2. Hydrodynamic Force Coefficients

Ali and Karim (2010) and Prasad *et al.* (2015) computed the hydrodynamic coefficients of lift and drag, represented on Fig. 6. A and B, along with a comparison with the present computations. Ali and Karim (2010) investigated the free-surface effects for h/c in the range 0.91 to 4, Prasad *et al.* (2015) studied the range 0.78 to 1.29, and the present work investigates a larger range of h/c values, from 0.25 to 4 ($h/c = 0.1$ was also simulated but the results were not considered reliable, as interfacial phenomena in heavy wave-breaking regime and when the foil upper surface gets dry are not accurately modeled). The results are very similar between the different studies, in particular regarding the lift coefficient:

- the difference on the lift coefficient is below 2% between our results and Ali and Karim (2010) results for $h/c > 2$ (and 3% for the specific condition of $h/c = 0.911$ when wave breaking starts occurring);
- the difference on the lift coefficient is below 4% between our results and Prasad *et al.* (2015) results for $0.78 < h/c < 1.29$.

Some discrepancies are visible on the drag coefficient:

- the difference on the drag coefficient is between 15% and 27% between our results and Ali and Karim (2010) results for $h/c > 2$ (and 42% for the specific condition of $h/c = 0.911$ when wave breaking starts occurring);
- the difference on the drag coefficient is below 12% between our results and Prasad *et al.* (2015) results for $h/c < 0.91$, but strongly increases to between 22% and 47% for $0.95 < h/c < 1.29$.

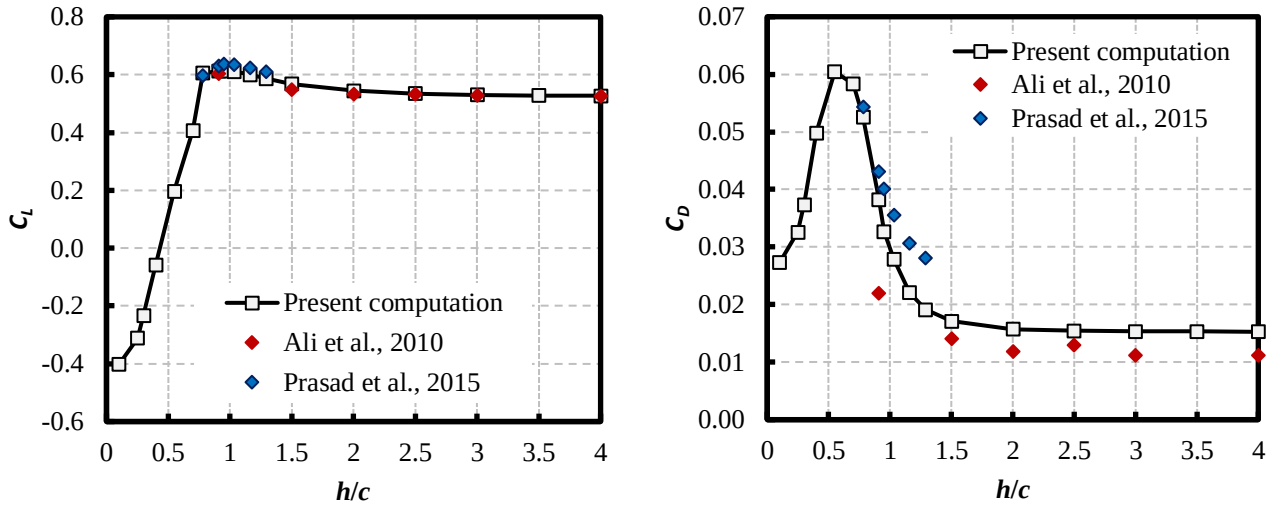

(A) **(B)**

Figure 6. Comparison of (A) lift coefficients and (B) drag coefficients between numerical data from Ali and Karim (2010) and Prasad et al. (2015) and the present computation. (Note that the results at $h/c = 0.1$ are not considered reliable.)

The evolution of the hydrodynamic coefficients with the different submergence depth shows three distinct regimes for the influence of the free-surface:

i) for high immersion, corresponding to $h/c > 2$, the free-surface is far from the immersed body and its effects are negligible. Indeed, there is almost no variation for the lift and drag coefficients, and they both tend towards the infinite depth (monofluid) value: total lift is 0.5197 for the infinite depth and 0.527 at $h/c = 4$ (1.4% difference), while total drag is 0.01496 for the infinite depth, and 0.01526 at $h/c = 4$ (2% difference);
ii) for moderate immersion, corresponding to $0.91 < h/c < 2$, the forces are affected by the free-surface; the amplitude of the waves above and downstream the foil increases as the immersion is reduced, but without wave breaking. The lift moderately increases (+12% between $h/c = 2$ and $h/c = 0.91$), while the drag drastically increases (+143% between $h/c = 2$ and $h/c = 0.91$);
iii) for low immersion, corresponding to $h/c < 0.91$, wave breaking occurs. Two "sub-regimes" may be observed: for $0.91 > h/c > 0.55$, the lift drops while the drag still increases, then for $h/c < 0.55$, both lift and drag drop.

3.3. Local Analysis: Pressure Fields

A deeper physical insight may be gained by looking at the pressure fields for the considered range of submergence depth to chord ratio (Fig. 7). For high immersion, corresponding to the first regime identified in the previous sub-section (i.e. $h/c > 2$), the pressure fields are similar to the infinite depth configuration (monofluid), and are not modified by a variation of the submergence depth (Fig. 7A); therefore, the lift and drag coefficients are quasi-constant. Then, when the influence of the free-surface on the body is no longer negligible, the pressure field is being altered.

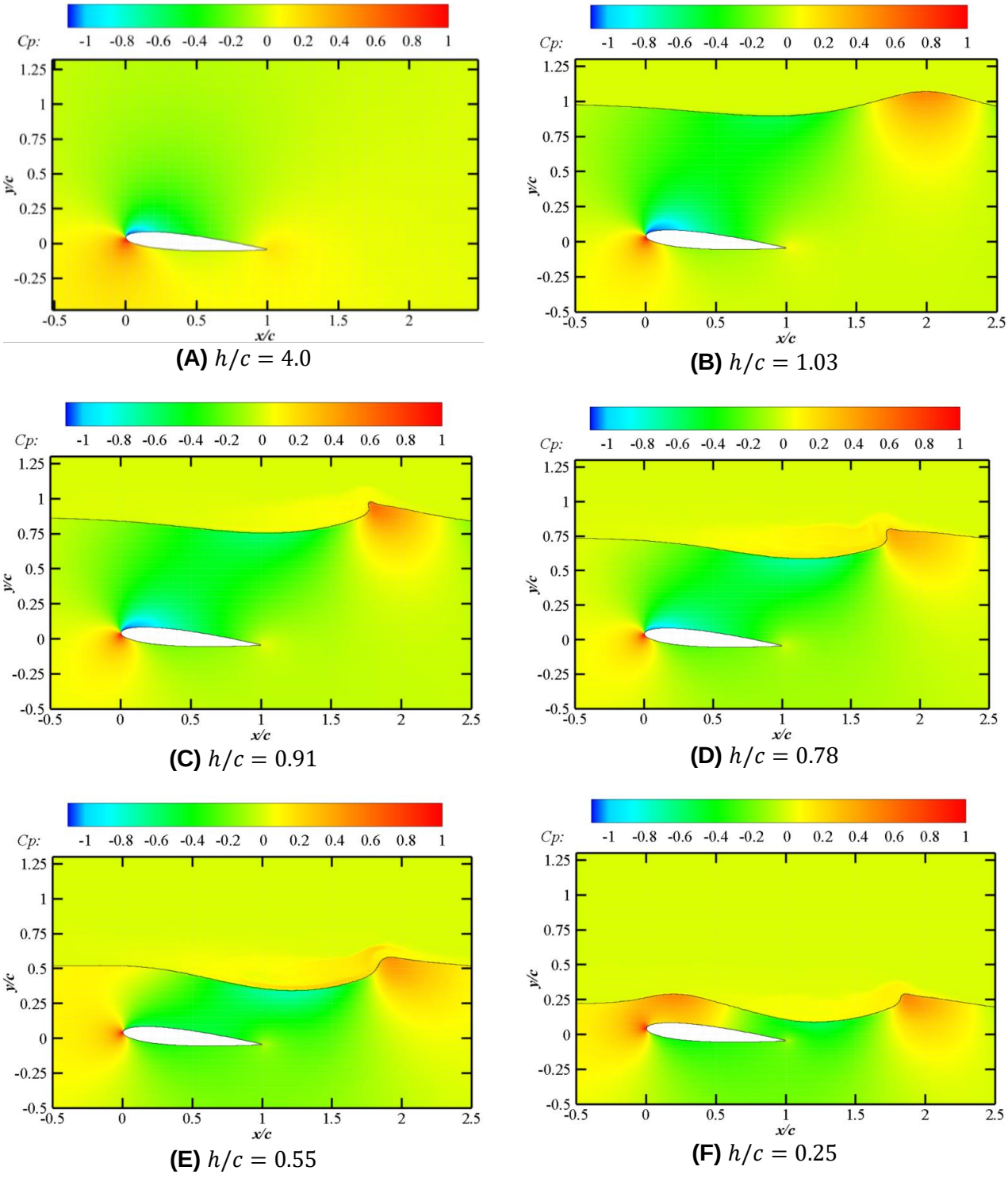

(A) $h/c = 4.0$ **(B)** $h/c = 1.03$

(C) $h/c = 0.91$ **(D)** $h/c = 0.78$

(E) $h/c = 0.55$ **(F)** $h/c = 0.25$

Figure 7. Hydrodynamic pressure field around the NACA0012 for different submergence depth to chord ratios, an angle of attack of 5° **and a chord-based Froude number of** 0.571**. (The hydrostatic pressure has been subtracted.)**

First, a comparison of Figure 7A (high immersion) and Figure 7B, C (moderate immersion) shows that the pressure on the suction side of the hydrofoil is lower for $h/c = 1.03$ and 0.911 than for $h/c = 4.0$. The flowing region above the foil is reduced by the trough in the free surface. This convergence effect is related to an acceleration of the flow, and then an even lower pressure on the suction side as in the well-known Venturi effect. This explains the increase in lift. The pressure

field on the pressure side seems almost unaffected by the presence of the free surface. For a lower immersion ($h/c = 0.78$ Fig. 7D, and lower), the high suction peak located near the leading edge is reduced, related to the decrease in lift. The effect of flow acceleration above the foil with convergence seems to level off (kind of blockage), the trough in the free surface moves downstream and the suction on the foil is reduced further. For the lowest immersion ($h/c = 0.25$ Fig. 7F), the pressure field is completely modified, with a high pressure zone developing on the first half of the upper side, associated with the presence of a wave crest above the leading edge, and the trough is pushed behind the foil. Moreover, the pressure is significantly decreased below the hydrofoil. This corresponds to the inversion of the lift with $C_L < 0$ (downward lift). It is noticeable that the stagnation point (red spot near the foil leading edge in Fig. 7) progressively moves up around the curve of the leading edge when the immersion is reduced from $h/c = 0.91$ down to $h/c = 0.25$, associated to the reduction and then inversion of the lift.

The deformation of the free surface becomes visible when $h/c < 2$ and increases progressively for lower values of the immersion. This deformation requires energy, and leads to a wave drag, which is the main reason for the increase in drag for decreasing immersion from $h/c = 2$ down to $h/c = 0.55$. The subsequent decrease in drag for $h/c < 0.5$ is not fully understood. As the amplitude of the following wave train is reduced, it may be conjectured that the wave drag decreases, but some energy is certainly dissipated in the wave breaking (and it is not certain that the heavy wave breaking is well represented by the simulation). Moreover, this change of trend on the drag occurs at the same submergence depth than the inversion in the direction of the lift, when the pressure field is completely modified.

4. CONCLUSIONS

This research constitutes the first step of an extensive investigation of free-surface effects on a submerged hydrofoil moving closely beneath a free-surface. A verification and validation study of a numerical model based on URANS modeling, closed by the classical *k-ω*-SST turbulence model and associated to a Volume of Fluid (VOF) model, is carried out on a two-dimensional NACA0012 at 5° angle of attack. Verification includes a mesh convergence study using an adaptive-grid-refinement technique, as well as a time convergence study on the free-surface deformation and hydrodynamic coefficients. The validation is done, first, on the free-surface deformation against the experimental work of Duncan (1983), for a range of submergence depth to chord ratios from 0.78 to 1.29. A good agreement is observed, although slightly less so for the more difficult configurations of wave-breaking. Moreover, the results are also compared with the simulations of Ali and Karim (2010) and Prasad *et al.* (2015), as they include the computation of the hydrodynamic coefficients of lift and drag that were not measured in the experimental work of Duncan. Similar trends are obtained, and quantitatively, the lift force agrees well (maximum discrepancies below 4%), and the drag shows more scatter (up to 47% at worse), but these other simulations consider a deeper water depth below the foil. Finally, a larger range of submergence depth to chord ratios is investigated, from 0.25 to 4.0, and an in-depth analysis of the hydrodynamic coefficients and pressure field surrounding the hydrofoil is presented, providing some new insights into the physics of free-surface effects on the behavior of hydrofoils. The free surface does not significantly affect the hydrodynamic forces for a submergence depth to chord ratio h/c higher than two. Closer to the free surface, the drag increases first slowly, then sharply up to more than threefold at h/c around 0.5. The lift slightly increases due to a Venturi effect above the foil until *h*/*c* around 1, and then decreases sharply and even changes to downward for $h/c < 0.5$ where the pressure field around the foil is totally modified. The study highlights the importance of considering the effect of the free surface proximity to correctly estimate the forces developed by hydrofoils used on foiling crafts. All in all, it is believed that the present model gives reliable results for h/c down to 1, and a reasonable approximation for lower submergence (more caution should apply when strong wave breaking occurs). Main limitations of the present work for real sailing applications are i) the bounded depth effect that is unlikely to occur in real sailing conditions and ii) the low Froude ($F_r = 0.571$) and Reynolds number of 159,000 values that are much lower than real sailing conditions ($F_r > 8$ and Reynolds number greater than 800,000). These limitations mainly come from the need to first validate the model against available

experimental data from the literature, before moving towards more realistic and difficult conditions. Now that the numerical framework is validated, we will address the case of infinite depth, which is more representative of actual sailing conditions. Further work will aim at a systematic investigation for different values of the Froude number and angle of attack, as well as considering deep water and 3D foil configurations.

5. ACKNOWLEDGEMENTS

This project is funded by the *Agence Nationale de La Recherche* (ANR) through grant n°ANR-19-STHP-0002 and uses HPC/AI resources from GENCI- [IDRIS] (Grant 2021-A10 [A0102A12500]) and HPC resources Datarmor. The authors are grateful to Tanguy Pallier at Ecole Navale and the technical services at GENCI, Datarmor and CADENCE / NUMECA for their support.

6. REFERENCES

Ali, A. and Karim, M. (2010). Numerical Study of Free Surface Effect on the Flow Around Shallowly Submerged Hydrofoil. *Martec 2010*, no. December: 1–6.

Bagué, A., Degroote, J., Demeester, T. and Lataire, E. (2021). Dynamic Stability Analysis of a Hydrofoiling Sailing Boat using CFD. *Journal of Sailing Technology,* 6(1), 58–72. https://doi.org/10.5957/jst/2021.6.1.58

Bal, S. (200)7. High-speed subermeged and surface-piercing cavitating hydrofoils, including tandem case. *Ocean Engineering,* 34(14-15), 1935-46. https://doi.org/10.1016/j.oceaneng.2007.03.007.

Buerman, T.M., Leehey, P. and Stilwell, J. J. (1953). An Appraisal of Hydrofoil Supported Craft. *Tansactions of the Society of Naval Architects And Marine Engineers,* 61, 242–79.

Daskovsky, M. (2000). The Hydrofoil in Surface Proximity, Theory and Experiment. *Ocean Engineering,* 27(10), 1129–59. https://doi.org/10.1016/S0029-8018(99)00032-3.

Duncan, J. H. (1983). The Breaking and Non-Breaking Wave Resistance of a Two-Dimensional Hydrofoil. *Journal of Fluid Mechanics,* 126, 507–20. https://doi.org/10.1017/S0022112083000294.

Eça, L. and Hoekstra, M. (2014). A Procedure for the Estimation of the Numerical Uncertainty of CFD Calculations Based on Grid Refinement Studies. *Journal of Computational Physics,* 262, 104–30. https://doi.org/10.1016/j.jcp.2014.01.006.

Faltinsen, O. M. (2005). Hydrofoil Vessels and Foil Theory. In *Hydrodynamics of High-Speed Marine Vehicles*, Cambridge, 165–220.

Filippas, E. S. and Belibassakis, K. A. (2014). Hydrodynamic Analysis of Flapping-Foil Thrusters Operating beneath the Free Surface and in Waves. *Engineering Analysis with Boundary Elements,* 41, 47–59. https://doi.org/10.1016/j.enganabound.2014.01.008.

Hoque, Md. A., Karim, MD. M. and Rahman, A. (2017). Simulation of Water Wave Generated by Shallowly Submerged Asymmetric Hydrofoil. *Procedia Engineering,* 194, 38–43. https://doi.org/10.1016/j.proeng.2017.08.114.

Hough, G. H. (1969). Froude Number Effect on Two-Dimensional Hydrofoils. *Journal of Ship Research,* 13(1), 53–60.

Karim, Md. M., Prasad, B. and Rahman, N. (2014). Numerical Simulation of Free Surface Water Wave for the Flow around NACA 0015 Hydrofoil Using the Volume of Fluid (VOF) Method. *Ocean Engineering,* 78, 89–94. https://doi.org/10.1016/j.oceaneng.2013.12.013.

Menter, F. R. (1994). Two-Equation Eddy-Viscosity Turbulence Models for Engineering Applications. *AIAA Journal,* 32(8), 1598–1605. https://doi.org/10.2514/3.12149

METHRIC. 2020. FINE/Marine - Theory Guide, V10.1.

Molland, A. F. (2008). Marine Vehicle Types. In *The Maritime Engineering Reference Book*, 43–74.

Ni, Z., Dhanak, M. and Su, T. C. (2021). Performance of a Hydrofoil Operating Close to a Free Surface over a Range of Angles of Attack. *International Journal of Naval Architecture and Ocean Engineering,* 13, 1–11. https://doi.org/10.1016/j.ijnaoe.2020.11.002.

Ozdemir, Y. H., Cosgun, T. and Barlas, B. (2021). Wave Field Generated by Finite-Span Hydrofoils Operating beneath a Free Surface. *Brodogradnja,* 72 (1): 145–67. https://doi.org/10.21278/brod72108.

Parkin, B. R., Perry, B. and Wu, T. Y. T. (1956). Pressure Distribution on a Hydrofoil Running near the Water Surface. *Journal of Applied Physics,* 27(3): 232–40. https://doi.org/10.1063/1.1722350.

Patterson, N. and Binns, J. (2022). Development of a Six Degree of Freedom Velocity Prediction Program for the foiling America's Cup Vessels. *Journal of Sailing Technology,* 7(1): 120–151. doi: https://doi.org/10.5957/jst/2022.7.6.151

Prasad, B., Hino, T. and Suzuki, K. (2015). Numerical Simulation of Free Surface Flows around Shallowly Submerged Hydrofoil by OpenFOAM. *Ocean Engineering,* 102, 87–94. https://doi.org/10.1016/j.oceaneng.2015.04.049.

Queutey, P. and Visonneau, M. (2007). An interface capturing method for free-surface hydrodynamic flows. *Computers and Fluids,* 36 (9), 1481-1510. https://doi.org/10.1016/j.compfluid.2006.11.007

Wackers, J., Deng, G. B., Guilmineau, E., Leroyer, A., Queutey, P., Visonneau, M., Palmieri, A. and Liverani, A. (2017). Can adaptive grid refinement produce grid-independent solutions for incompressible flows? *Journal of Computational Physics,* 344, 364-380. https://doi.org/10.1016/j.jcp.2017.04.077

Nan, X. and Dracos, V. (2009). Performance analysis of 3D hydrofoil under free-surface. *Ocean Engineering,* 34(8-9), 1257-64. https://doi.org/10.1016/j.oceaneng.2006.05.008.

Yeung, R. W. and Bouger, Y. C. (1979). A hybrid integral-equation method for steady twodimensional ship waves. *International Journal for Numerical Methods in Engineering,* 14, 317-336.